JOURNAL OF SOLID STATE CHEMISTRY 81, 217–229 (1989)

A Study of a New Incommensurate Phase in the System $SrMn_{1-x}Co_xO_{3-y}$

P. D. BATTLE AND T. C. GIBB*

School of Chemistry, The University, Leeds LS2 9JT, England

AND R. STRANGE

Daresbury Laboratory, Daresbury, Warrington WA4 4AD, England

Received January 3, 1989

The oxygen-deficient system $SrMn_{1-x}Co_xO_{3-y}$ ($0 \leq x \leq 1$) has been studied by X-ray and neutron powder diffraction, magnetic susceptibility, ^{57}Fe Mössbauer spectroscopy, and EXAFS techniques. Three new phases have been obtained, the most significant being an incommensurate phase for $0.40 \leq x \leq 0.55$ which is believed to be closely related to the family of perovskite structures with hexagonal symmetry. However, the EXAFS data show the existence of some as yet unidentified structural features which are not found in perovskites, for example a Co–Co distance of ~2.8 Å. The Mn cations occupy an environment which is significantly different from that of the Co cations. At high cobalt content ($x \sim 0.8$) and high temperatures the system adopts a pseudocubic perovskite structure, with corner-shared polyhedra, which transforms on slow cooling to a poorly defined "hexagonal" phase containing face- and edge-shared polyhedra, similar to H-$Sr_2Co_2O_{5+z}$. There is evidence to suggest that these "hexagonal" phases may also be incommensurate. © 1989 Academic Press, Inc.

Introduction

The solid-solution $SrMn_{1-x}Co_xO_3$ ($0 \leq x \leq 1$), which can be prepared under high pressures of oxygen, adopts the cubic perovskite structure for all values of x at room temperature (*1–3*). The available crystallographic and magnetic data reveal that the Co^{4+} ($3d^5$) ions are in the low-spin (t_{2g}^5, $S = 1/2$) configuration in $SrCoO_3$ and at the cobalt-rich end of the solid solution, but that for $x < =0.7$ there is a transformation to the high-spin ($t_{2g}^3 e_g^2$, $S = 5/2$) configuration.

The normal form of $SrMnO_3$ as prepared in air is the hexagonal 4H-$SrMnO_3$, and we have recently reported a reinvestigation of the structural and magnetic properties of this compound (*4*). The cobalt end-member of the solid solution, when prepared in air rather than in oxygen, is oxygen deficient. The highly reduced composition $SrCoO_{2.5}$ (or $Sr_2Co_2O_5$) can exist in two forms. *B*-$Sr_2Co_2O_5$ contains high-spin Co^{3+} (d^6, $S = 2$) at both the octahedral and tetrahedral sites of a brownmillerite structure, derived from the simple cubic perovskite by an ordering of oxygen vacancies along ⟨110⟩ directions, whereas H-$Sr_2Co_2O_5$ is an ill-defined "hexagonal" phase. We have recently studied these two polymorphs by Mössbauer spectroscopy (*5*) and by EXAFS spectroscopy (*6, 7*). Direct evidence was found for the existence of face-sharing CoO_6 octahedra in

* To whom correspondence should be addressed.

0022-4596/89 $3.00
Copyright © 1989 by Academic Press, Inc.
All rights of reproduction in any form reserved.

H-$Sr_2Co_2O_5$, and it appears likely that there is, at least in part, a transformation to the low-spin $S = 0$ state of Co^{3+}. Oxidation to give H-$Sr_2Co_2O_{5+z}$ takes place with retention of the same "hexagonal" structure, but there is evidence in the EXAFS data for edge-sharing of polyhedra, as well as face-sharing. The brownmillerite structure is only stable for samples having $z \simeq 0$.

In this paper we report an investigation of the oxygen-deficient system $SrMn_{1-x}Co_xO_{3-y}$ by X-ray and neutron powder diffraction, Mössbauer and EXAFS spectroscopy, and magnetic susceptibility techniques, and we demonstrate the existence of a new and novel incommensurate solid-solution phase.

Experimental

Samples of $SrMn_{1-x}Co_xO_{3-y}$ were prepared from spectroscopic-grade $SrCO_3$, MnO_2, and Co_3O_4. Materials weighed in the appropriate stoichiometric ratios were ground together in a ball mill and pressed into a pellet, which was fired in a platinum crucible at 1200°C for 72 hr and cooled at 100°C hr^{-1} to 500°C before removing from the furnace. Initial characterization was by X-ray powder diffraction recorded with a Philips diffractometer using nickel-filtered Cu$K\alpha$ radiation. The heating cycle was usually repeated several times to ensure homogeneity. Aliquots were also annealed at 1200°C and quenched in air onto a metal plate. An attempted estimation of oxygen content by iodometric analysis was not successful, and approximate values for the oxygen content were obtained from the weight loss observed during the initial heating. Selected preparations were repeated in a similar manner, except that $^{57}Fe_2O_3$ was used to substitute ^{57}Fe for ~1% of the Mn/Co cations.

Magnetic susceptibility data were measured as a function of temperature for $80 < T < 300$ K using a Newport Instruments Gouy balance. Mössbauer data were collected on the ^{57}Fe-doped samples in the temperature range $4.2 < T < 290$ K using a ^{57}Co/Rh source matrix held at room temperature; isomer shifts were determined relative to the spectrum of metallic iron. Neutron diffraction data were collected at room temperature using the powder diffractometer D2b at ILL Grenoble, operating at a wavelength of 1.594 Å. The sample was contained in a 12-mm-diameter vanadium can. Each scan over the angular range $0 < 2\theta < 160°$ lasted for ~4 hr using a 2θ step size of 0.05°.

Room-temperature EXAFS spectra were recorded at the Co K-edge (1.60811 Å, 7.710 keV) and the Mn K-edge (1.89636 Å, 6.538 keV) using the Daresbury synchrotron radiation source, operating at an energy of 2.0 GeV and a maximum beam current of 220 mA. Data were recorded in the transmission mode on station 7.1, with the finely ground, undiluted samples held between strips of adhesive tape. A Si(111) double-crystal order-sorting monochromator was used to substantially reduce the harmonic content of the monochromatic beam. Established procedures were used to extract the EXAFS oscillations from the absorption data (*8*). The background-subtracted EXAFS was then converted into k-space and weighted by k^3 in order to compensate for the diminishing amplitude at high k due to the decay of the photoelectron wave. The data were Fourier filtered to include only the first three (or four) shells, a cut-off which can be made without introducing large truncation errors and which is not complicated by overlapping Fourier transform shells. Analysis of the Fourier-filtered EXAFS was carried out using the nonlinear least-squares program EXCURV88 (*9*). An ab-initio approach was used to calculate the atomic phase-shifts, as previously described (*6, 7, 10*). The reliability of the phase-shifts for the Co system has already been established (*6*). The calculated

phase-shifts for Mn, as both absorbing atom and backscattering atom, and for Sr, as backscattering atom, were checked by simulating the EXAFS of the crystallographically characterized compound 4H-$SrMnO_3$. We estimate the following levels of accuracy in our refinements: coordination number ±50%, Debye–Waller factor ±50%, and radii ±0.02 Å. These are estimates arising from imperfect transferability of phase shifts and the fitting procedure described below. Statistical fitting errors are far smaller.

Results and Discussion

Samples in the solid-solution $SrMn_{1-x}Co_xO_{3-y}$ were prepared initially at increments of 0.1 in x, although additional compositions were added subsequently. It was found that there were several distinct regions in the system, and these will now be considered in turn.

The region $0 < x < 0.40$

For $x = 0.1$, 0.2, and 0.3 the product of the initial firing gave an X-ray powder pattern which contained lines from 4H-$SrMnO_3$ and a new phase (which for reasons set out below will be referred to as the icH-phase) A close comparison of the relative intensities of the strongest lines in both patterns showed a composition dependence that was linear upon x. It was apparent that little or no cobalt enters the 4H-$SrMnO_3$ lattice during a reaction in air, and that the amount of 4H-$SrMnO_3$ extrapolates to zero at $x = 0.40$. The sample for $x = 0.40$ seemed to contain a very small trace of 4H-$SrMnO_3$, which was not removed after seven firing cycles. Inhomogeneity in the reaction mixture probably produces some 4H-$SrMnO_3$ as an initial product which may be difficult to remove by further annealing. There was also some evidence to support the existence of weak lines in the icH-pattern coincident with those of $SrMnO_3$. The lower limit of the icH-phase is believed to be $x = 0.40$.

The Region $0.40 < x < 0.55$ (The icH-Phase)

The new icH-phase was also obtained as a single-phase material for $x = 0.42$, 0.45, 0.50, and 0.55 and is considered to exist over the range $0.40 < x < 0.55$. Very sharp X-ray powder patterns were observed. Chemical analysis for oxygen by redox methods proved difficult because of the comparative insolubility of the phase in acid. Observations of the weight loss on initial firing for the different samples were self-consistent and gave compositions ranging from $SrMn_{0.60}Co_{0.40}O_{2.61}$ to $SrMn_{0.45}Co_{0.55}O_{2.52}$ (the error in y is estimated to be ±0.03). Thus there is a substantial reduction from the +4 oxidation state found in 4H-$SrMnO_3$, and to a large degree both cobalt and manganese are nominally in a +3 oxidation state. Quenching rapidly from 1200°C appeared to give the identical material to that observed by cooling slowly in air, as judged by X-ray powder diffraction.

A detailed analysis of the X-ray powder patterns might have proved impossible were it not for a fortunate coincidence. The pattern for $x = 0.40$ was eventually indexed with some confidence as a hexagonal cell with a long c-axis. The parameters were $a = 5.531$ [$= \sqrt{2}a_p$ where a_p is the cell parameter of a cubic perovskite] and $c = 56.59$ Å [$= (25/3)\sqrt{3}a_p$]. The c parameter corresponds closely to a 25H-structure, which is not inconsistent with the cation ratio (3Mn + 2Co). However, examination of the patterns for larger x revealed that this interpretation was too simplistic. Although the positions of the $hk0$ reflections (and the value of a) were almost independent of the composition, many of the hkl reflections moved substantially, but to both higher *and* lower d-spacings. The phase is clearly hexagonal, but incommensurate along the c-axis (hence the adopted name, icH-phase).

Neutron diffraction data for samples with $x = 0.42$ and 0.55 were useful in confirming the existence of some of the weaker lines in the X-ray patterns and also showed some new lines, but because of the better inherent angular resolution, the analysis was largely completed using the X-ray data. However, the reflections observed in both the X-ray and neutron diffraction data could be encompassed within the final interpretation.

A satisfactory analysis of the observed d-spacings of all five patterns was achieved using a four-dimensional relationship of the form

$$\frac{1}{d^2} = \frac{4(h^2 + hk + k^2)}{3a^2} + \frac{(l + j\delta)^2}{c^2},$$

where j is the integer index (positive or negative) for the incommensuration along c, c is the axis length for the subcell, and c/δ is the axis length for the supercell. The cell parameters are given in Table I. The a and c parameters remain almost independent of composition and correspond to $\sqrt{2} \times 3.91$ and $(5/3)\sqrt{3} \times 3.94$ Å respectively; i.e., the subcell is a 5H-structure. The δ parameter changes monotonically with composition, and accidentally (?) has a value close to 0.2 at $x = 0.40$, generating an apparent 25H-cell.

The observed d-spacings of 24 of the best resolved lines are shown in Table II. Ignoring the negligible change in a, the change in $1/d^2$ between two compositions $x = p$ and $x = q$ can be written as

$$\begin{aligned}\Delta(1/d^2) &= (1/c^2)[(l + j\delta_p)^2 - (l + j\delta_q)^2] \\ &= (1/c^2)(\delta_p - \delta_q)[2lj + j^2(\delta_p + \delta_q)] \\ &= \beta[2lj + j^2(\delta_p + \delta_q)],\end{aligned}$$

where $\beta = (1/c^2)(\delta_p - \delta_q)$. The last column in Table II tabulates $10^5 \times \beta$ (which should be a constant) from a comparison of the sample with $p = 0.40$ and $q = 0.55$. Despite the large error in measuring small line shifts, the numbers obtained have a broadly similar magnitude and above all the correct *sign* for the j index adopted in each case. The cell parameters in Table I were refined using the data in Table II (except for those values in parentheses which are from broadened or asymmetric lines). The remaining weak or unresolved lines could then be assigned, but unless the movement with composition of a line could be observed clearly, the assignments for higher angles were often ambiguous. They are therefore not tabulated here.

It would be imprudent to assume that this structural characterization is correct in all details because of the limited one-dimensional nature of the powder X-ray data. Clearly a three-dimensional characterization by electron diffraction is highly desirable; unfortunately we do not have the necessary facilities available. Nevertheless, the incommensurate nature of the icH-phase is beyond doubt. Possible causes of the incommensuration will be discussed below.

The reciprocal magnetic susceptibility values, $1/\chi$, between 78 and 300 K for $x = 0.42$, 0.45, 0.55, and 0.40 (doped with ^{57}Fe) are shown in Fig. 1. Above 200 K the dependence is close to linear, the slope at 300 K leading to lower limits for the effective magnetic moments of between 4.0 and 4.5 Bohr magnetons (for $x = 0.40$ and 0.55, respectively), and Curie–Weiss temperatures of circa −220 K. This behavior indicates

TABLE I

THE CELL PARAMETERS FOR THE icH-PHASE OF $SrMn_{1-x}Co_xO_{3-y}$ AS A FUNCTION OF COMPOSITION

x	y	a	c	δ
0.40	0.39	5.531	56.59(25H)	—
		5.527	11.32	0.194
0.42	0.42	5.523	11.31	0.194
0.45	0.45	5.529	11.33	0.176
0.50	0.46	5.528	11.35	0.148
0.55	0.48	5.525	11.32	0.135

TABLE II

OBSERVED *d*-SPACINGS FOR $SrMn_{1-x}Co_xO_{3-y}$

				0.40					0.55		
						0.42	0.45	0.50			
h	*k*	*l*	*j*	obs	calc	obs	obs	obs	obs	calc	$10^5 \times \beta$
0	0	2	−1	6.282	6.265	6.281	6.204	(6.05)	(6.03)	—	—
1	0	0	0	4.778	4.786	4.768	4.794	4.797	4.795	4.785	—
1	0	2	−1	3.807	3.804	3.803	3.791	3.758	(3.74)	—	—
1	0	3	−1	3.084	3.084	3.082	3.078	3.061	3.046	3.046	47(3)
1	1	0	0	2.762	2.763	2.760	2.767	2.767	2.763	2.763	—
1	0	4	0	2.436	2.436	2.434	2.437	2.440	—	—	—
2	0	0	0	2.395	2.393	2.392	2.394	2.396	2.393	2.392	—
2	0	2	−1	2.238	2.236	2.234	2.235	2.228	2.224	2.226	71(12)
1	1	3	+1	2.181	2.179	2.179	2.185	2.190	2.191	2.194	30(7)
2	0	2	+1	2.168	2.171	2.168	2.172	2.180	2.183	2.181	64(10)
2	0	3	−1	2.058	2.058	2.057	2.055	2.051	2.045	2.046	51(8)
0	0	6	−2	2.017	2.016	2.014	2.007	1.991	1.975	1.977	44(2)
1	1	4	0	1.976	1.977	1.974	1.980	1.983	—	—	—
2	0	4	−1	—	—	1.864	1.864	1.860	1.857	1.853	—
1	0	6	−2	1.857	1.858	1.856	1.851	1.836	1.826	1.826	43(2)
2	1	2	+1	1.706	1.707	1.706	1.708	1.711	1.710	1.712	35(10)
2	1	3	−1	1.650	1.651	1.649	1.650	1.648	1.645	1.644	43(7)
1	1	6	−2	1.628	1.629	1.628	1.623	1.614	1.606	1.607	44(2)
3	0	0	0	1.595	1.596	1.594	1.595	1.596	1.594	1.595	—
2	0	6	−2	1.542	1.542	1.541	1.537	1.530	1.522	1.523	47(2)
3	0	2	+1	1.524	1.524	1.523	1.526	1.527	1.527	1.527	36(9)
3	0	3	+1	1.456	1.455	1.454	1.458	1.458	1.459	1.459	31(9)
3	0	4	0	1.390	1.390	1.389	1.391	1.392	1.391	1.390	—
2	2	0	0	1.382	1.382	1.381	1.382	1.382	1.381	1.381	—

essentially antiferromagnetic spin interactions at low temperatures. The gradual increase in the gradient of $1/\chi : T$ below 200 K probably represents the onset of short-range near-neighbor magnetic couplings, with a corresponding change in the average cation magnetic moment. However, we do not believe that the change in slope represents a transition to a phase with long-range weak ferromagnetism because the magnetic susceptibility showed no significant field dependence over the measured temperature range.

The highly reduced nature of the phase suggests high-spin $Co^{3+}(d^6)$ and $Mn^{3+}(d^4)$ as the primary oxidation states, both of which have a spin-only effective moment of 4.9 Bohr magnetons. Significant amounts of low-spin Co^{3+} ($S = 0$) can be excluded. Any oxidation is likely to produce $Mn^{4+}(d^3\ S = 3/2)$, with a moment of 3.9 Bohr magnetons, in preference to Co^{4+} and this is broadly in accord with the observed moments.

The magnetic properties were also investigated by Mössbauer spectroscopy on the samples with $x = 0.40$ doped with 1% ^{57}Fe. The spectra as a function of temperature are shown in Fig. 2. At 290 K the spectrum comprises a sharp quadrupole doublet *A* (chemical shift $\delta = 0.37$, quadrupole splitting $\Delta = 1.23$ mm sec^{-1}) and a broad singlet *B* ($\delta = 0.26$ mm sec^{-1}). At 190 K the singlet *B* is considerably broadened, and at 170 K a magnetic hyperfine splitting broadened by relaxation is evident. This has begun to

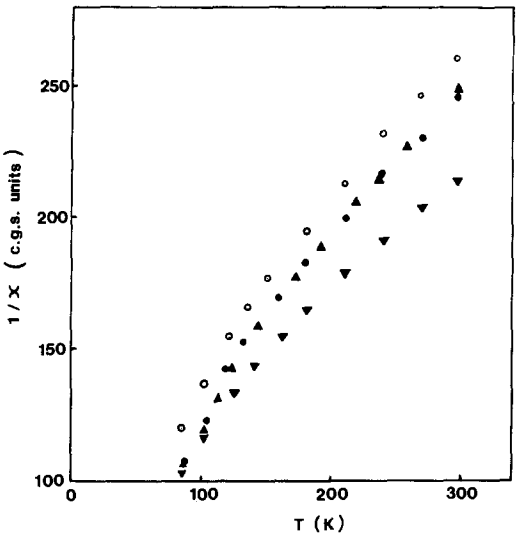

FIG. 1. The reciprocal susceptibility, $1/\chi$, as a function of temperature, T, for $SrMn_{1-x}Co_xO_{3-y}$ with x = 0.42 (●), 0.45 (▲), 0.55 (▼), and 0.40 (doped with ^{57}Fe (○)).

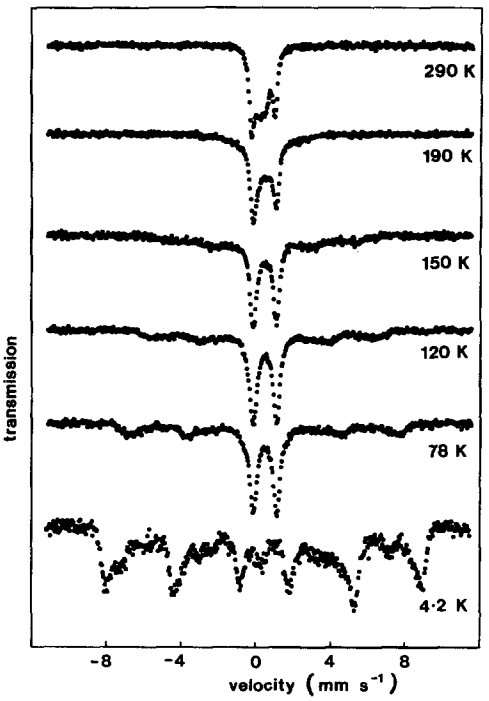

FIG. 2. The Mössbauer spectrum as a function of temperature for $SrMn_{0.60}Co_{0.40}O_{2.61}$ doped with ^{57}Fe.

sharpen to a static splitting at 78 K, ultimately reaching a saturation flux density of circa 52 T at 4.2 K. The quadrupole doublet *A* remains apparently unaffected by magnetic broadening down to at least 78 K, and although at 4.2 K a large magnetic field has emerged, there is still evidence for some measure of relaxational collapse. Component *B*, which shows magnetic splitting below about 200 K, correlates well with the observed susceptibility data and confirms that a change in magnetic behavior does indeed occur below this approximate temperature. However, the spectra are inconsistent with a simple long-range magnetic order below 200 K. We believe that components *A* and *B* derive from two different iron sites in the phase which show different relaxation effects. Component *B* may well be associated with short-range spin interactions. The shift of doublet *A* is characteristic of Fe^{3+} in 6-coordination to oxygen, and is significantly more positive than for component *B* which is intermediate in shift between values observed (*11*) for 4- and 6-coordination to oxygen in related perovskites. There is therefore some evidence to associate component *B* with iron in 5-coordinated sites. The large quadrupole splitting of component *A* is noteworthy for an Fe^{3+} ion. It is possible that these are face-sharing octahedral sites with a high axial anisotropy.

EXAFS spectroscopy was used to probe the local environments of both transition-metal cations in this incommensurate phase. Figures 3a and 3b show the observed and calculated Fourier-filtered cobalt EXAFS and their Fourier transforms for the sample $SrMn_{0.55}Co_{0.45}O_{2.55}$. Qualitatively, these spectra are typical of all compositions in the icH-phase, and represent an averaged summation over all the cobalt sites present. In the absence of any other structural data on these materials, the approximate averaged occupation numbers of the various coordination shells were deter-

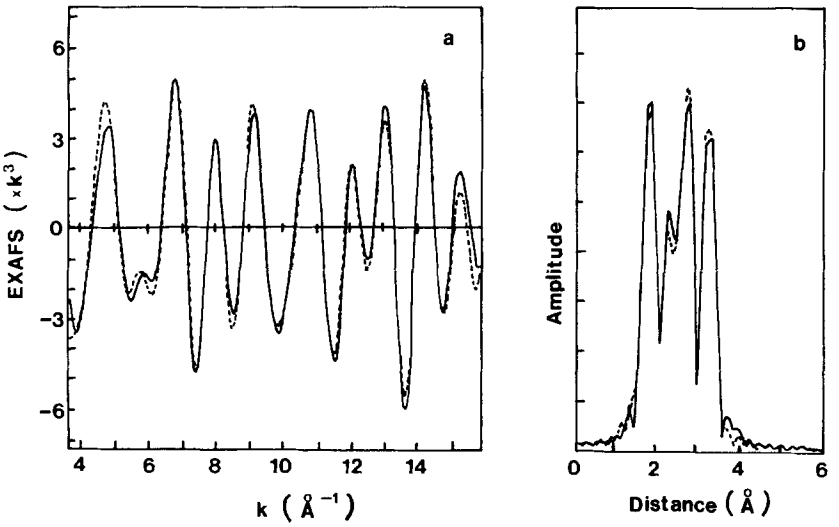

FIG. 3. The observed and calculated (dotted line) Fourier-filtered cobalt EXAFS (a) and their Fourier transforms (b) for the sample $SrMn_{0.55}Co_{0.45}O_{2.55}$.

mined in preliminary fits by allowing the coordination number and Debye–Waller factor to refine. The former were then held constant at the nearest half-integer value during final refinements of the shell radius and the Debye–Waller factor, thus leading to the rather high estimated error of 50% discussed above. The refined structural parameters are listed in Table III. The first coordination shell, with two unresolved components at distances of 1.93 and 2.14 Å from the central cobalt atom, is assigned as an oxygen shell, whereas the second shell, at a distance of 2.56 Å is a Co/Mn shell. The former assignment is entirely consistent with the coordination geometry expected in a mixed-metal oxide, and the magnitude of the shell radius supports the proposal that the cobalt ions are in a high-spin state.

The assignment of the second shell as a Co/Mn shell is in accord with our previous study (*6*) of H-$Sr_2Co_2O_5$ where we interpreted the data in terms of face-sharing CoO_6 octahedra, with a Co–Co distance of 2.46 Å. We believe that face-sharing polyhedra are also present in large numbers in $SrMn_{1-x}Co_xO_{3-y}$, but because of the similarity in the X-ray scattering powers of Mn and Co we are unable to distinguish between Co–Co and Co–Mn units. The radial distances and coordination numbers reported in Table III for the third and fourth coordination shells are in very close agreement with those reported previously (*7*) for the partially oxidized sample H-$SrCoO_{2.63}$. They are assigned to a Mn/Co shell and a strontium shell, respectively, and the third shell distance of 2.87 Å is consistent with the presence of edge-sharing octahedra. However, the occupation number of the

TABLE III

REFINED STRUCTURAL PARAMETERS FOR $SrMn_{0.55}Co_{0.45}O_{2.55}$ FROM Co-K EXAFS DATA

Atom type	Average coordination number	$2\sigma^2$ (Å²)	Radial distance (Å)
O	2	0.004	1.93
O	2	0.010	2.14
Co/Mn	1	0.015	2.56
Co	1	0.006	2.87
Sr	1	0.006	3.21

third shell (best refined as containing only Mn/Co) varies considerably over the composition range $0.40 < x < 0.55$, rising to a value of 6 for $x = 0.55$. Even allowing for the large errors associated with the refined values of the coordination number, we have no structural explanation for this increase, which was accompanied by a lengthening of the shell radius to 3 Å. In view of these difficulties experienced in producing a convincing model for the third shell, we shall limit ourselves to a qualitative description of the environment beyond the second shell, noting only the apparent similarity between the Co environment in $SrMn_{1-x}Co_xO_{3-y}$ ($0.40 < x < 0.55$) and that found in H-$Sr_2Co_2O_{5+z}$.

The analysis of the corresponding manganese EXAFS data is more straightforward. Figures 4a and 4b show the observed and calculated Fourier-filtered manganese EXAFS and their Fourier transforms for the sample $x = 0.45$. The first coordination shell is occupied by five oxygen atoms at a distance of 1.88 Å, and the second shell again consists of a transition metal cation at a distance of 2.53 Å. The observation of this shell in both the Co and Mn EXAFS data proves that both metals occupy, at least in part, face-sharing polyhedra. The refined shell radii, occupation numbers, and Debye–Waller factors are listed in Table IV. The third shell is assigned to a strontium atom at 3.21 Å; there is no evidence for the existence of edge-sharing polyhedra containing manganese.

It is interesting to note that although we have only attempted to analyze data out to ~3.2 Å, the Fourier transform of the Co EXAFS showed features at greater distances whereas that of the Mn EXAFS did not. This implies that there is a greater degree of disorder around the Mn cations than is found about the Co cations. One possible explanation is that anion vacancies concentrate around the former thus leading to local displacements and consequently a more rapid fall off in the Fourier transform of the observed EXAFS.

The Region $0.55 < x < 1.00$

The X-ray powder diffraction pattern for slow-cooled samples with $x = 0.6$ and $x = 0.7$ showed clear evidence for the contin-

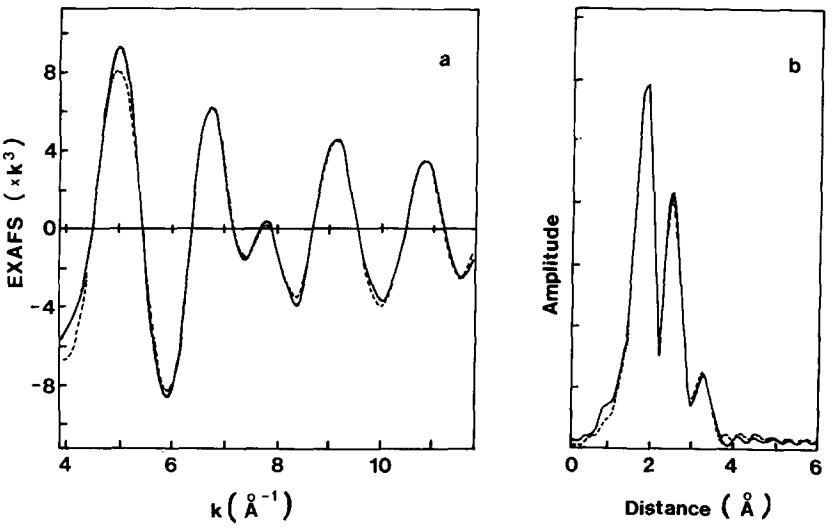

FIG. 4. The observed and calculated (dotted line) Fourier-filtered manganese EXAFS (a) and their Fourier transforms (b) for the sample $SrMn_{0.55}Co_{0.45}O_{2.55}$.

TABLE IV

REFINED STRUCTURAL PARAMETERS FOR $SrMn_{0.55}Co_{0.45}O_{2.55}$ FROM Mn-K EXAFS DATA

Atom type	Average coordination number	$2\sigma^2$ (Å^2)	Radial distance (Å)
O	5	0.015	1.88
Co/Mn	1	0.008	2.53
Sr	1	0.016	3.21

ued existence of the icH-phase with *d*-spacings apparently the same as for $x = 0.55$, but with additional lines from a second phase. At $x = 0.8$ and $x = 0.9$ the icH-phase was absent, and it became clear that the new phase was isostructural with the ill-defined "hexagonal" phase H-$Sr_2Co_2O_{5+z}$. Weight loss measurements indicated that the sample with $x = 0.80$ had the composition $SrMn_{0.2}Co_{0.8}O_{2.64}$. It is worth noting that figures for the oxygen content of the $Sr_2Co_2O_{5+z}$ system determined by both weight loss and chemical analysis were in good agreement, thus lending credence to the use of weight-loss data for the analysis of the Mn/Co system.

It is well known that H-$Sr_2Co_2O_5$ transforms to B-$Sr_2Co_2O_5$ at high temperatures, and in an attempt to prepare B-$SrMn_{1-x}Co_xO_{2.5}$, samples for $x = 0.6$, 0.7, 0.8, and 0.9 were quenched from 1200°C in air. The X-ray pattern for $x = 0.9$ resembled a mixture of a brownmillerite and a cubic perovskite; that for $x = 0.8$ was a cubic perovskite with a unit cell size of circa 3.87 Å, although the {211} reflection in particular showed noticeable splitting. A similar sample doped with ^{57}Fe was clearly noncubic with a formula from weight-loss measurements of $SrMn_{0.2}Co_{0.8}O_{2.60}$, there being no detectable gain in weight upon slow cooling in air to give the "hexagonal" form. For $x = 0.6$ and 0.7 the product was a mixture of the icH-phase and the perovskite. We shall focus our attention on the pseudocubic sample with $x = 0.8$: it

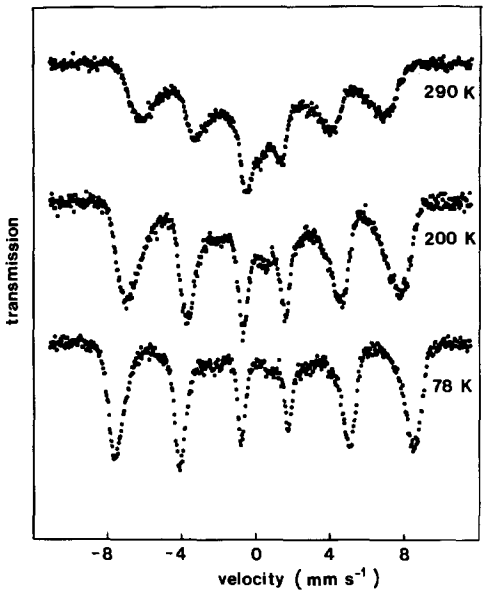

FIG. 5. The Mössbauer spectrum as a function of temperature for pseudocubic $SrMn_{0.20}Co_{0.80}O_{2.60}$ doped with ^{57}Fe.

is apparent that this compound shows a phase transformation that is different from that shown by $Sr_2Co_2O_5$.

The Mössbauer spectra for the $x = 0.8$ quenched, pseudocubic, doped sample (Fig. 5) show magnetic behavior at room temperature and no evidence at 78 K for the characteristic spectrum of a brownmillerite in which ordered vacancies produce both octahedral and tetrahedral sites (the spectrum for doped B-$Sr_2Co_2O_5$ is shown in Ref. (*6*)). Although a cubic X-ray pattern could result from a microdomain texture of a brownmillerite lattice (*11*, *12*), the Mössbauer data clearly show that this is not the case in the present instance.

The Mössbauer spectra for the $x = 0.8$ slow-cooled, "hexagonal" doped sample (Fig. 6) are completely different and strongly resemble those for the icH-phase. The main feature is a quadrupole doublet ($\delta = 0.36$, $\Delta = 1.23$ mm sec^{-1} at 295 K). This feature was also recorded previously in doped "hexagonal" $Sr_2Co_2O_{5+z}$ ($\delta = 0.38$,

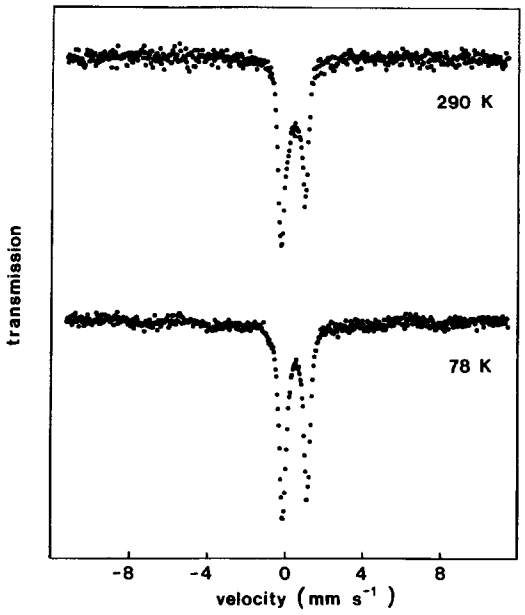

FIG. 6. The Mössbauer spectrum as a function of temperature for "hexagonal" $SrMn_{0.20}Co_{0.80}O_{2.60}$ doped with ^{57}Fe.

$\Delta = 1.22$ mm sec^{-1}), suggesting a common structural relationship between all three phases. The remaining contributions to the spectra have an isomer shift of about 0.09 mm sec^{-1} at 295 K and suggest the existence of higher oxidation states. At 78 K the quadrupole doublet is retained but there is now evidence for a very weak magnetic hyperfine splitting, again reminiscent of the behavior shown by the icH-phase.

The cobalt EXAFS spectra of both the slow-cooled and the quenched samples of $SrMn_{0.2}Co_{0.8}O_{2.64}$ were recorded as described above. Figures 7a and 7b show the observed and calculated Fourier-filtered EXAFS and their Fourier transforms for the slow-cooled sample. The refined structural parameters are listed in Table V. The first coordination shell is assigned to six oxygen atoms at a distance of 1.89 Å and there is clear evidence for a cobalt neighbor at 2.44 Å. The third shell occurs at a distance of 2.84 Å, consistent with the possible existence of edge-sharing polyhedra, but again we are unable to offer a convincing structural explanation of the data beyond a radius of 2.5 Å; indeed the assignment of backscattering species beyond 3.0 Å is uncertain. However, these EXAFS spectra provide further evidence that the local environment around the Co atoms is very simi-

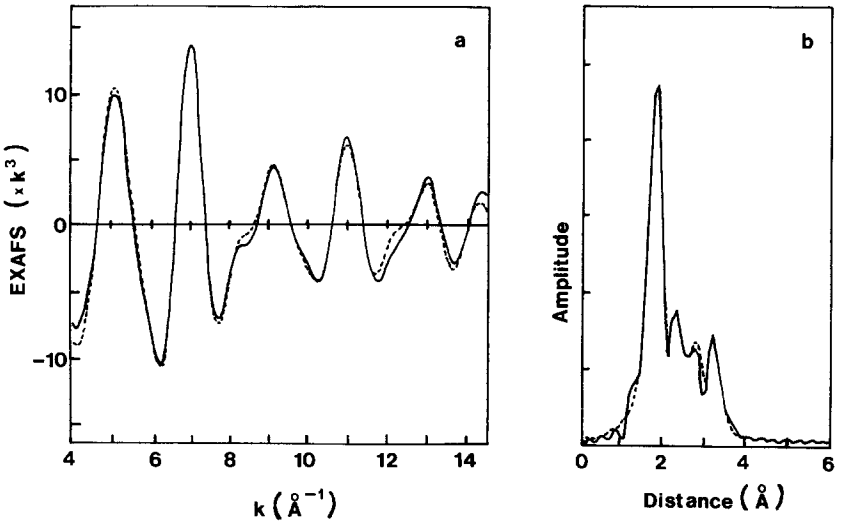

FIG. 7. The observed and calculated (dotted line) Fourier-filtered cobalt EXAFS (a) and their Fourier transforms (b) for the "hexagonal" sample of $SrMn_{0.20}Co_{0.80}O_{2.64}$.

TABLE V

REFINED STRUCTURAL PARAMETERS FOR $SrMn_{0.2}Co_{0.8}O_{2.64}$ (SLOW-COOLED) FROM Co-K EXAFS DATA

Atom type	Average coordination number	$2\sigma^2$ (Å^2)	Radial distance (Å)
O	6	0.009	1.89
Co/Mn	1	0.013	2.44
Co/Mn	1	0.010	2.84
Sr	1	0.012	3.21
Co	2	0.018	3.26

TABLE VI

REFINED STRUCTURAL PARAMETERS FOR $SrMn_{0.2}Co_{0.8}O_{2.64}$ (QUENCHED) FROM Co-K EXAFS DATA

Atom type	Average coordination number	$2\sigma^2$ (Å^2)	Radial distance (Å)
O	2	0.005	1.81
O	2	0.009	1.94
O	1	0.017	2.13
Sr	4	0.030	3.21
Co/Mn	4	0.012	3.89
O	4	0.006	4.04

lar in all three of the icH-phase, "hexagonal" $Sr_2Co_2O_{5+z}$, and "hexagonal" $SrMn_{0.2}Co_{0.8}O_{2.64}$ (the present sample).

Figures 8a and 8b show the observed and calculated EXAFS spectra and their Fourier transforms for the pseudocubic quenched sample of $SrMn_{0.2}Co_{0.8}O_{2.64}$. These spectra are clearly very different from those described above. The refined parameters listed in Table VI can be interpreted in terms of a distorted perovskite structure with a cubic unit cell parameter a_p of ~3.9 Å. The first coordination shell once again comprises five oxygen atoms, but the second shell now consists of strontium atoms at a distance of 3.21 Å, somewhat shorter than the distance of 3.38 Å ($\sqrt{3}a_p/2$) expected in an ideal cubic perovskite. There is no evidence for short Co–Co distances, a result that implies that only corner-sharing polyhedra are present in this phase. The shell at 3.89 Å represents the Co atoms distant a_p from the central atom, and the contribution at 4.04 Å comes from the

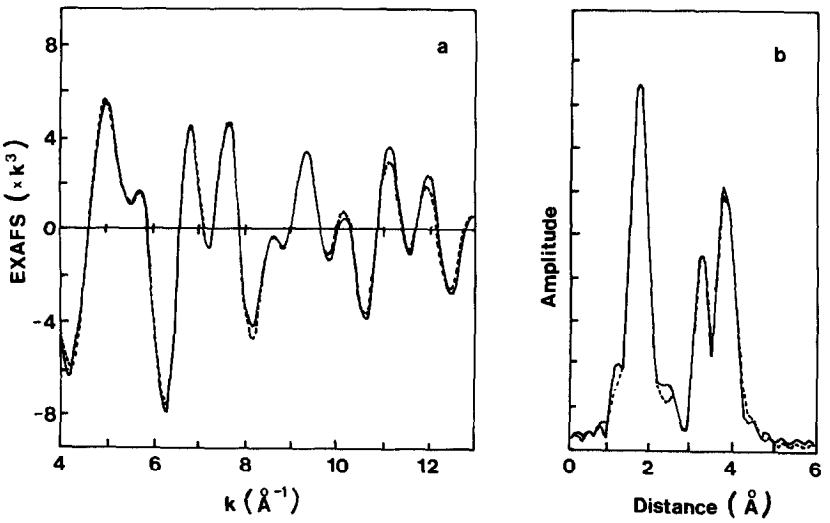

FIG. 8. The observed and calculated (dotted line) Fourier-filtered cobalt EXAFS (a) and their Fourier transforms (b) for the pseudocubic sample of $SrMn_{0.20}Co_{0.80}O_{2.64}$.

second oxygen shell, ideally $\sqrt{5}a_p/2$ distant from the central atom. The shift in the positions of the Sr and O shells indicates that the local environment of the Co atoms in this phase deviates from that expected in an ideal perovskite structure, as is to be expected in a compound with such a high concentration of vacancies in the anion sublattice. However, it is apparent that the crystal structure of the quenched sample is closer to that of a cubic perovskite than to that of the "hexagonal" phase. Our attempts to record EXAFS spectra at the Mn absorption edge for samples in this composition range were unsuccessful because of the low Mn concentration.

The Nature of the Incommensurate Phase

The most significant result to come out of this work is the discovery of the icH-phase in the $SrMn_{1-x}Co_xO_{3-y}$ system. There is some evidence to suggest that it is closely related to the perovskite family of structures, but with some as yet unidentified and novel structural features which are not found in perovskites, for example, edge-sharing polyhedra (or an alternative scheme which accounts for a Co–Co distance of ~2.8 Å).

The reasons for an incommensuration in crystals are many and varied (*13*), and it is not a trivial problem to characterize the icH-phase. The subcell of the incommensurate lattice has dimensions corresponding to those expected for a 5H-perovskite. There is only one conventional stacking sequence for a 5H-structure, *hhccc*, which results in stacks of three face-sharing octahedra, linked by two layers of corner-sharing octahedra. The average number of face-sharing cation neighbors would be 0.8. The EXAFS data are completely inconsistent with a simple ordering of Mn and Co cations onto face- and corner-sharing sites, respectively. However, it is clear that the Mn cations occupy an environment that is significantly different from that of the Co cations, as exemplified by the absence of a 2.8 Å metal–metal distance in the Mn EXAFS, and therefore the 5H-lattice is an inadequate model. It is possible that this partial cation ordering may be responsible for the formation of an incommensurate phase; the systematic variation of δ with x suggests that the effect is perhaps governed by the cation sublattice. Certainly a highly disordered intergrowth of two (or more) structural features along the c-axis could lead to an incommensurate lattice (*14*).

However, we are unable to exclude a model in which δ is determined by the ordering of oxygen vacancies, although the ordering of vacancies would presumably be related to the cation distribution, and the vacancy concentration does not change very much with x. Examples are known of very high vacancy concentrations in hexagonal perovskites without any overall disruption of the stacking sequence. In 6H-$BaFeO_{2.79}$ there is a higher concentration of vacancies in the hexagonally stacked BaO_3 layers than in the cubic stacked layers (*15*), but electron microscopy reveals a very regular lattice with only the occasional stacking fault (*16*). In 12H-$BaCoO_{2.6}$ the vacancies partially order into cubic stacked BaO_3 layers to effectively convert corner-sharing octahedra into tetrahedra (*17, 18*), but once again the lattice remains regular.

There is some evidence from electron microscope images to show (*19*) that a small amount of Ta substituted into 2H-$BaMnO_3$ can produce a highly irregular stacking sequence along the c-axis. The corresponding diffraction patterns appear to show satellites in the c^* direction which may be indicative of incommensuration, and we feel that this system warrants a more detailed examination.

Mössbauer spectroscopy has shown that the cation sites are very similar in H-$Sr_2Co_2O_{5+z}$, the icH-phase, and "hexagonal" Sr $Mn_{0.2}Co_{0.8}O_{2.60}$. The magnitude of the hy-

perfine field (46.5 T) observed in the first compound at 4.2 K led us (*5*) to suggest that it derived from a cation site with a coordination number lower than six, and the temperature dependence of the Mössbauer spectrum indicated that the hyperfine splitting was caused by slow relaxation rather than by long-range magnetic ordering. The appearance of the Mössbauer spectra described above is not inconsistent with this interpretation. A disordered intergrowth along the *c*-axis may well inhibit long-range magnetic order. The apparent similarity between the icH-phase and the "hexagonal" phases has caused us to look again at X-ray powder diffraction patterns recorded on our samples of H-$Sr_2Co_2O_{5+z}$. Although we are still unable to index these patterns in a satisfactory way, the shift in peak positions with composition leads us to suggest that this phase may also be incommensurate.

Acknowledgments

We acknowledge the SERC for financial support. The EXAFS experiments described above were performed under the auspices of the Daresbury Laboratory EXAFS service.

References

1. H. Taguchi, M. Shimada, F. Kanamura, M. Koizumi, and Y. Takeda, *J. Solid State Chem.* **18,** 299 (1976).
2. H. Taguchi, M. Shimada, M. Koizumi, and F. Kanamura, *J. Solid State Chem.* **35,** 246 (1980).
3. H. Taguchi, M. Shimada, and M. Koizumi, *J. Solid State Chem.* **40,** 42 (1981).
4. P. D. Battle, T. C. Gibb, and C. W. Jones, *J. Solid State Chem.* **74,** 60 (1988).
5. P. D. Battle and T. C. Gibb, *J. Chem. Soc. Dalton Trans.*, 667 (1987).
6. P. D. Battle, T. C. Gibb, and A. T. Steel, *J. Chem. Soc. Dalton Trans.*, 2359 (1987).
7. P. D. Battle, T. C. Gibb, and A. T. Steel, *J. Chem. Soc. Dalton Trans.*, 83 (1988).
8. EXCALIB and EXBACK programs available from Daresbury Laboratory.
9. N. Binsted, S. Gurman, and J. Campbell, "Daresbury Laboratory EXCURV88 Program" (1988).
10. N. Binsted, S. L. Cook, J. Evans, G. N. Greaves, and R. J. Price, *J. Amer. Chem. Soc.* **109,** 3669 (1987).
11. P. D. Battle, T. C. Gibb, and S. Nixon, *J. Solid State Chem.* **73,** 330 (1988).
12. T. C. Gibb, *J. Solid State Chem.* **74,** 176 (1988).
13. T. Hanssen and A. Janner, *Adv. Phys.* **36,** 519 (1987).
14. L. A. Bursill and G. Grzinic, *Acta Crystallogr. Sect. B* **36,** 2902 (1980).
15. A. J. Jacobson, *Acta Crystallogr. Sect. B* **32,** 1087 (1976).
16. J. L. Hutchison and A. J. Jacobson, *J. Solid State Chem.* **20,** 417 (1977).
17. A. J. Jacobson and J. L. Hutchison, *J. Solid State Chem.* **35,** 334 (1980).
18. A. J. Jacobson and J. L. Hutchison, *J. C. S. Chem. Commun.*, 116 (1976).
19. H. Shibahara, *J. Solid State Chem.* **66,** 116 (1987).